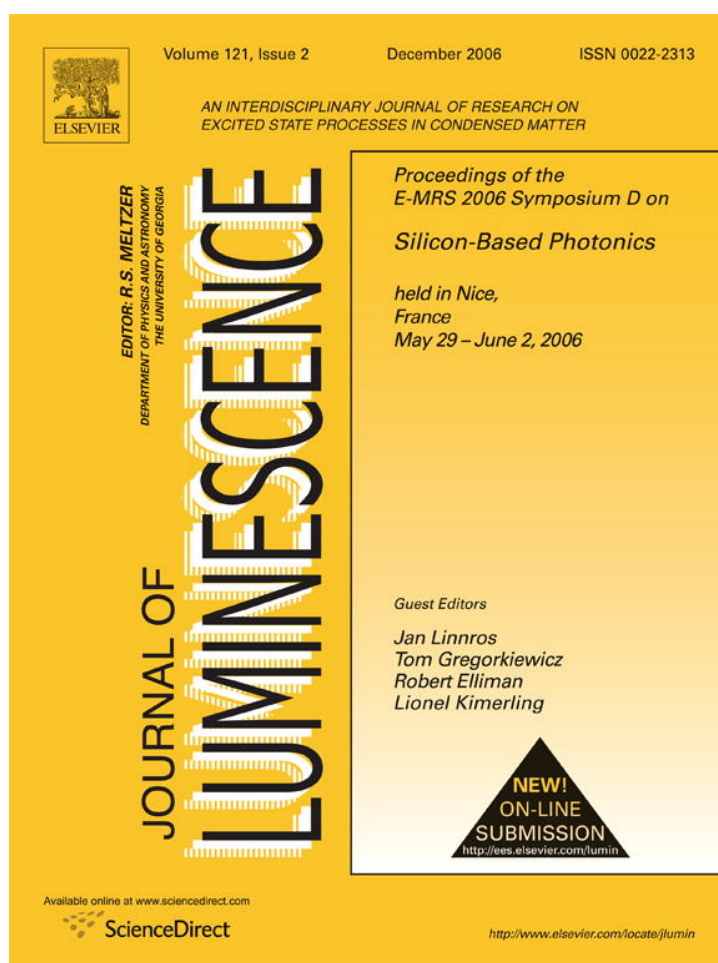


Provided for non-commercial research and educational use only.
Not for reproduction or distribution or commercial use.



This article was originally published in a journal published by Elsevier, and the attached copy is provided by Elsevier for the author's benefit and for the benefit of the author's institution, for non-commercial research and educational use including without limitation use in instruction at your institution, sending it to specific colleagues that you know, and providing a copy to your institution's administrator.

All other uses, reproduction and distribution, including without limitation commercial reprints, selling or licensing copies or access, or posting on open internet sites, your personal or institution's website or repository, are prohibited. For exceptions, permission may be sought for such use through Elsevier's permissions site at:

<http://www.elsevier.com/locate/permissionusematerial>



Silicon nanocrystals in silica—Novel active waveguides for nanophotonics

P. Janda^a, J. Valenta^{a,*}, T. Ostatnický^a, E. Skopalová^b, I. Pelant^b,
R.G. Elliman^c, R. Tomasiunas^d

^aDepartment of Chemical Physics & Optics, Faculty of Mathematics and Physics, Charles University, Prague, Czech Republic

^bInstitute of Physics, Academy of Sciences of the Czech Republic, Prague, Czech Republic

^cElectronic Materials Engineering Department, Research School of Physical Sciences and Engineering, Australian National University, Canberra, Australia

^dInstitute of Materials Science and Applied Physics, Vilnius University, Vilnius, Lithuania

Available online 7 September 2006

Abstract

Nanophotonic structures combining electronic confinement in nanocrystals with photon confinement in photonic structures are potential building blocks of future Si-based photonic devices. Here, we present a detailed optical investigation of active planar waveguides fabricated by Si⁺-ion implantation (400 keV, fluences from 3 to 6 × 10¹⁷ cm⁻²) of fused silica and thermally oxidized Si wafers. Si nanocrystals formed after annealing emit red-IR photoluminescence (PL) (under UV-blue excitation) and define a layer of high refractive index that guides part of the PL emission. Light from external sources can also be coupled into the waveguides (directly to the polished edge facet or from the surface by applying a quartz prism coupler). In both cases the optical emission from the sample facet exhibits narrow polarization-resolved transverse electric and transverse magnetic modes instead of the usual broad spectra characteristic of Si nanocrystals. This effect is explained by a theoretical model which identifies the microcavity-like peaks as leaking modes propagating below the waveguide/substrate boundary. We present also permanent changes induced by intense femtosecond laser exposure, which can be applied to write structures like gratings into the Si-nanocrystalline waveguides. Finally, we discuss the potential for application of these unconventional and relatively simple all-silicon nanostructures in future photonic devices.

© 2006 Elsevier B.V. All rights reserved.

PACS: 78.67.Bf; 42.79.gn; 81.07.Bc

Keywords: Nanocrystals; Waveguide; Silicon; Photonics

1. Introduction

Research on silicon-based photonics is motivated by the aim to combine integrated electronic and photonic structures on a single silicon chip. Silicon quantum dots or nanocrystals (Si-NCs) have attracted much attention due to their strong photoluminescence (PL) [1] and have been used to demonstrate silicon-based light-emitting diodes [2,3]. Ensembles of Si-NCs can also be employed to fabricate active optical waveguides [4–8] that exhibit spectral filtering of the Si-NC PL emission, if the refractive

index profile is properly designed. The occurrence of narrow (~10 nm), polarization-dependent emission lines was reported by Khriachtchev et al. [4] for Si/SiO₂ waveguides and by our group [5,9] for samples containing Si-NC prepared by Si⁺-implantation into silica slabs. In our previous papers we explained the unexpected waveguiding properties using a model based on substrate leaking modes of a lossy waveguide [10,11].

In this work we compare the propagation of the intrinsic luminescence from Si-NCs with that of external light coupled into the waveguides. This knowledge is crucial for pump-and-probe measurements (e.g. optical gain) and potential application as photonic devices (modulators, amplifiers etc.). In addition we show permanent changes

*Corresponding author. Tel.: +420 221911272; fax: +420 221911249.
E-mail address: jan.valenta@mff.cuni.cz (J. Valenta).

induced by femtosecond laser exposure which can be applied to write 2D structures (gratings etc.) into the Si-nanocrystalline waveguides with sub-micron resolution.

2. Experimental methods

Samples used in this study were prepared by Si⁺-ion implantation into 1 mm thick Infrasil (refractive index $n_s = 1.455$) slabs with polished surfaces and edges, and into SiO₂ layers (about 5 μm thick) prepared by thermal oxidation of Si wafers. An implantation energy of 400 keV and ion fluences ranging between 3.0 and $6.0 \times 10^{17} \text{ cm}^{-2}$ were used to fabricate the slab waveguides. In order to form Si nanocrystals the samples were annealed for 1 h at 1100 °C in an N₂ ambient and then passivated for 1 h at 500 °C in forming gas (5% H₂ in N₂).

The implanted layer acts as an asymmetric planar waveguide. The profile of the refraction index depends not only on the implantation energy and fluence but also on the annealing conditions. Although the annealing temperatures, ambients and durations were nominally the same, various sets of samples were annealed in different laboratories and furnaces. Possible variations in the thermal history and levels of oxidation lead to apparent differences in refraction index for nominally identical samples (here, Figs. 2–4 present results from one set of samples and another set with lower refraction index is shown in Figs. 5–7). In order to numerically model the optical properties of particular samples the refraction index profiles were measured separately for each implanted sample. This was done by measuring infrared transmission spectra (see Fig. 2B) and fitting the interference fringes assuming an asymmetric double-Gaussian refraction index profile. The maximum of the profile is typically about 600 nm below surface with a half width of about 300 nm. The peak refraction index has a value as high as 2 for the highest implantation fluence [11]. The diameter of nanocrystals in the samples is estimated to be between 4 and 6 nm using Raman scattering (not shown here) [11].

PL was excited by a continuous wave He–Cd laser (325 nm, excitation intensity $\sim 0.3 \text{ W/cm}^2$). The sample was placed on a rotatable x – y – z stage. A microscope with numerical aperture (NA) of 0.075 (i.e. an angular resolution of about 8.6°) was used to collect light and send it to a detection system consisting of an imaging spectrograph (Jobin Yvon Triax 190) with a CCD camera (Hamamatsu C4880) [9]. All measurements were performed at room temperature and all PL spectra were corrected for the system response.

The coupling of external light into the waveguides was achieved in two ways (Fig. 1):

(a) Prism coupling of light from the upper surface of the sample. Light from the Xe or halogen lamp was collimated into a quartz prism. For better optical contact between the prism and sample an immerse liquid (index of refraction $n = 1.515$) was dropped between the contact surfaces.

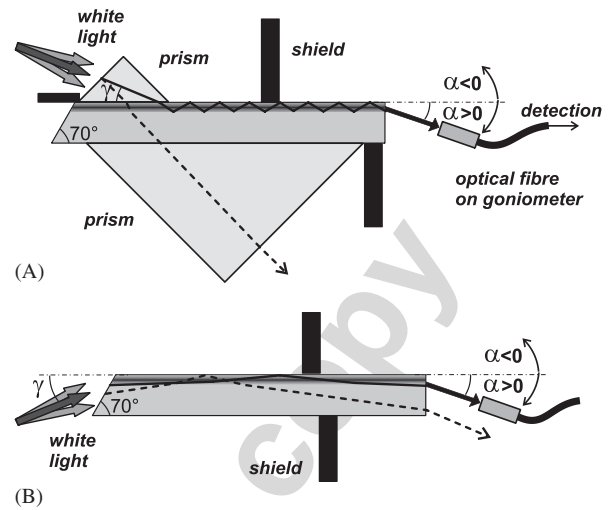


Fig. 1. Two experimental arrangements for coupling of external light into a waveguide sample: (A) coupling through a quartz prism on the upper sample surface. The second prism below sample is used to inhibit the back reflection of light not coupled into the waveguide; (B) focused light directed on the truncated edge of a sample. In both cases light leaving the opposite edge of sample is collected with an optical fiber and sent to a spectrometer. Sketches not to scale.

(b) Direct coupling into the truncated facet (Fig. 1B). The edge of the sample was polished at angle of about 70° in order to separate light refracted to the higher-index waveguide from light entering lower-index substrate. Here a warm-white LED was used as a convenient light source. The angle of incidence γ was between 15° and 30° with respect to the plane of implanted layer. The divergence of incident light was about 10°.

In both external-light-coupling set-ups the signal is collected by an optical fiber (detection NA ~ 0.008) and guided to the entrance slit of the imaging spectrometer Jobin Yvon Triax 320 (with the low-dispersion grating of 100 grooves/mm). Spectra are detected with the PI-Max intensified CCD (Princeton Instruments).

3. Results and discussion

3.1. Transmission spectra of Si-NC layers

The color of the Si-NC waveguide layers is yellow-brown with the optical density increasing with implantation fluence. The corresponding absorbance spectra are plotted in Fig. 2A (they are measured in a direction perpendicular to the nanocrystal plane using a UV-VIS double beam spectrometer (Hitachi U-3300), the non-implanted area of a silica slab being employed as a reference). The absorption edge has approximately exponential shape. In infrared spectral region several interference fringes are observed (Fig. 2B) which are used to model refraction index profile (see above).

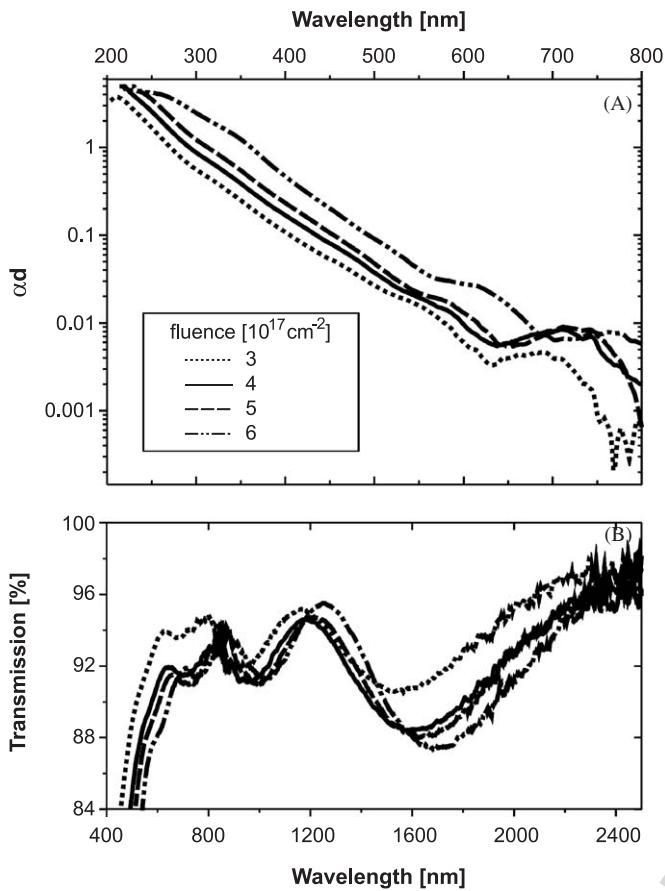


Fig. 2. (A) Absorption spectra of the samples implanted with fluences from 3 to 6 × 10¹⁷ cm⁻². A non-implanted area of the fused silica slab was used as a reference. (B) Infrared transmission spectra of the same samples. Interference fringes are used to calculate refractive index profiles.

3.2. PL of active planar waveguides

The PL spectra of the active planar waveguides have very different shape depending on the experiment geometry. Two arrangements are used: (i) the light is collected in a direction roughly perpendicular to the sample plane (this is a conventional PL arrangement) or (ii) in the direction close to parallel to the waveguide plane (i.e. from the sample facet–waveguide arrangement)—see inset in Fig. 3. In the former geometry the PL spectra are always broad with a peak around 830 nm, typical of oxide-passivated Si NCs with mean diameter ~5 nm. On the other hand, the waveguide geometry reveals narrow (down to 10 nm) spectral features with a high degree of linear polarization.

Figs. 3A and B show PL spectra of implanted oxide layers (on Si substrates) measured in directions perpendicular and parallel to the layer, respectively. The conventional PL (Fig. 3A) is modulated by deep interference fringes due to high reflectivity of the Si substrate. The facet-PL (Fig. 3B) is not affected by interference; instead a relatively narrow band is observed, the position of which depends on implantation fluence (i.e. refractive index profile). This peak shows partial linear polarization

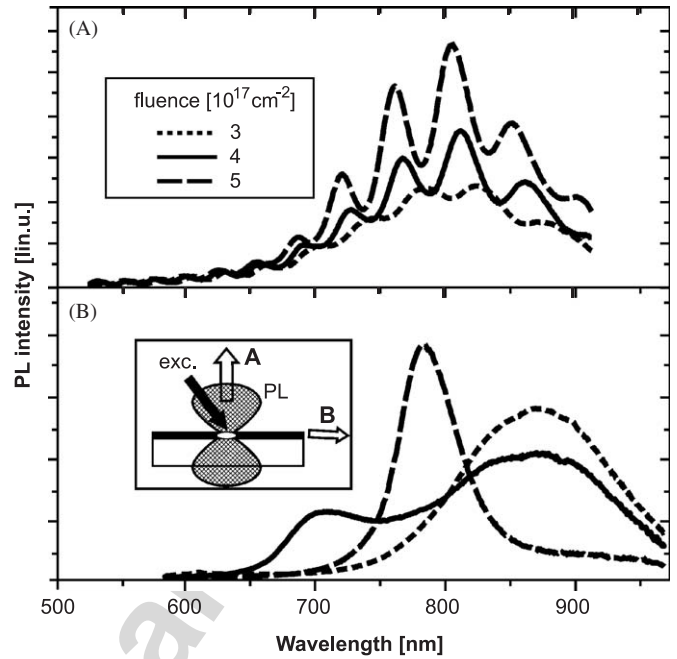


Fig. 3. PL spectra of SiO₂ layers on Si substrates implanted with fluences of 3, 4, and 5 × 10¹⁷ cm⁻². (A) PL detected in direction perpendicular to the layer. (B) PL detected in direction parallel to the layer (from the facet). The inset illustrates the experimental arrangement.

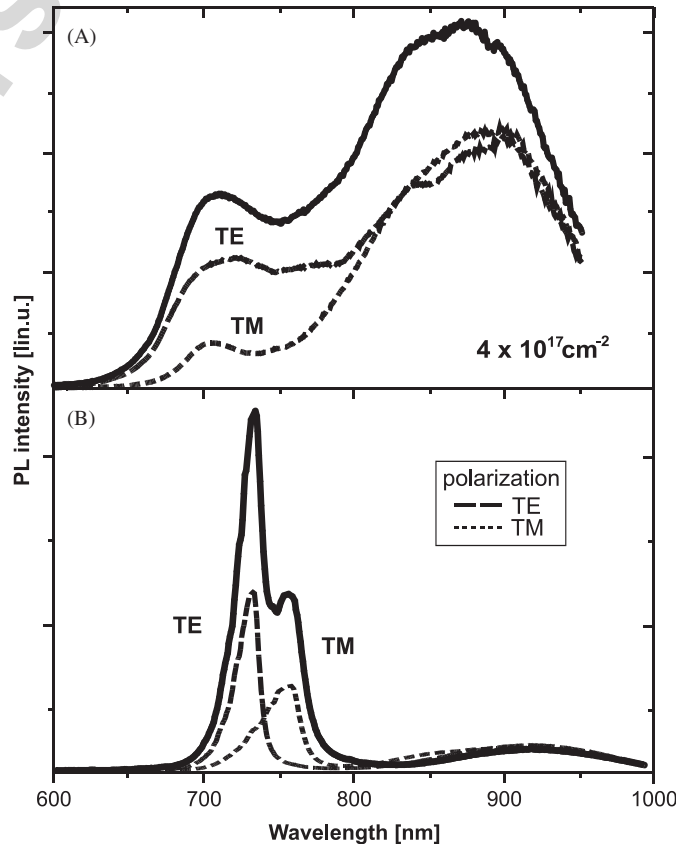


Fig. 4. PL spectra of 4 × 10¹⁷ cm⁻² layers measured in edge geometry without polarizer (solid line) or with a linear polarizer parallel (TE, dashed line) or perpendicular to the waveguide plane (TM, dotted line). The upper panel (A) concerns SiO₂ layers on Si substrate, while the lower panel (B) is for implanted fused silica slab.

(Fig. 4A). Under identical conditions (of both fabrication and PL-experiment) the facet-PL features are much better resolved in implanted silica slabs (Fig. 4B). Here a clear splitting of the narrow PL peak into two peaks with polarization parallel (transverse electric TE or *s* mode) and perpendicular (transverse magnetic TM or *p* mode) to the Si-NC waveguide plane is observed. The following discussion is restricted to implanted fused silica slabs where the TE/TM splitted modes are nicely resolved.

PL spectra of other set of five samples prepared by implantation to fluences of 4.0, 4.5, 5.0, 5.5, and $6.0 \times 10^{17} \text{ cm}^{-2}$ are plotted in Fig. 5. The upper spectra in Fig. 5A represent PL collected from the plane of implanted layers, while the lower PL spectra with TE/TM double-peaks are collected from the facet at angle $+5^\circ$ ($\text{NA}_{\text{det}} = 0.075$). An angle-resolved facet PL spectra from the layer implanted with dose of $6 \times 10^{17} \text{ cm}^{-2}$ are plotted in Fig. 5B and the polar representation of their integrated intensity is shown in Fig. 5C. The TE/TM split doublets shift

to longer wavelength with increasing implantation dose. The facet PL has a very narrow emission cone with the maximum slightly shifted closer to substrate ($\alpha \geq 0^\circ$) (Figs. 1B and C).

3.3. Theoretical model of the mode structure—radiative substrate modes

The surprising PL observations reported above do not correspond to simple waveguiding in ideal transparent waveguide which should transmit a continuous spectrum of guided modes up to a cut-off wavelength [12]. The cut-off for the first order modes of our waveguides can be estimated to lie above $\sim 1500 \text{ nm}$. Consequently, the waveguides should transmit the entire 600–900 nm band emitted by Si-NCs, which is clearly not the case. There are two possible explanations:

- (i) *Delocalized guided modes*: Let us assume wavelength-dependent losses in the waveguide, then those modes

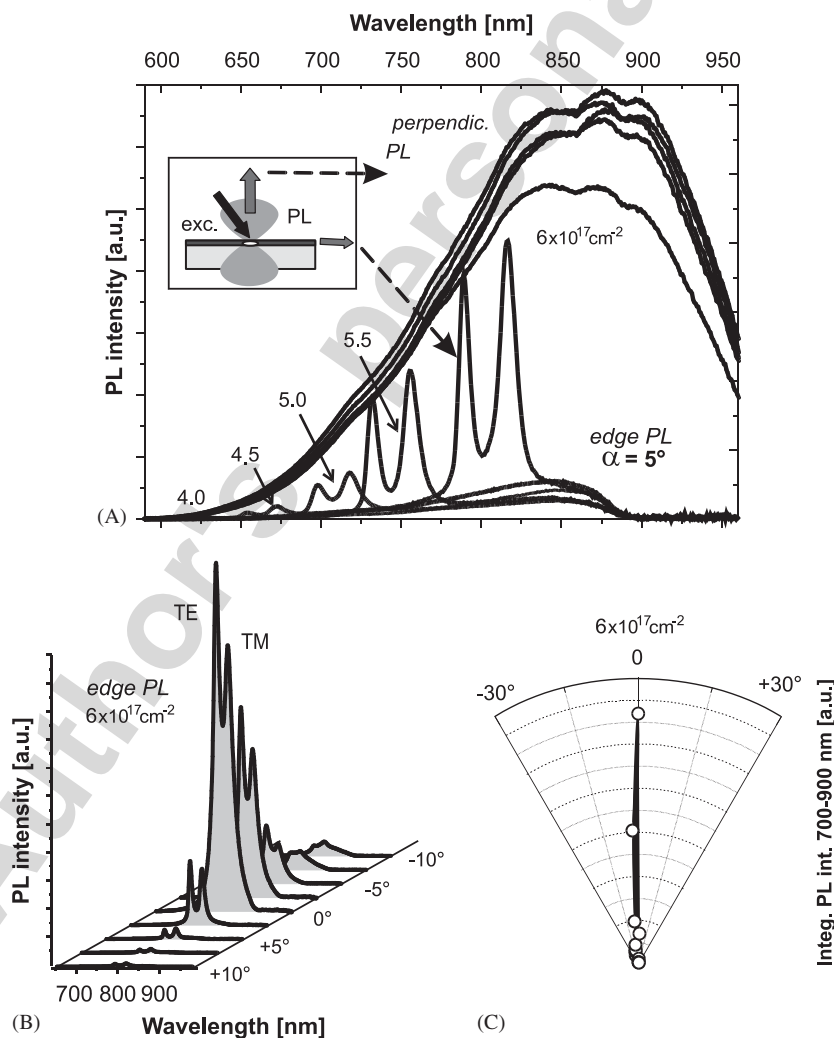


Fig. 5. PL spectra of five fused silica slabs implanted to fluences of $4\text{--}6 \times 10^{17} \text{ cm}^{-2}$. (A) Upper curves (a single wide band) correspond to PL emitted in a direction perpendicular to the waveguide, while lower spectra with doublet peaks are facet-PL detected in a direction $\alpha = 5^\circ$ (a sketch of the experimental arrangement is shown in the inset). (B) Angle resolved facet PL spectra of the sample $6 \times 10^{17} \text{ cm}^{-2}$. (C) Polar representation of integrated PL intensity of angle resolved facet spectra from the panel B. Most of the PL intensity is emitted in a direction close to 0° .

(wavelengths) that undergo the smallest losses will be advantaged. These are likely those modes that are “weakly guided” with a strongly delocalized electric field. Such modes propagate basically as planar waves in the substrate [13]. Ray optics describes these modes by an angle of incidence θ that is *greater than* but very close to the critical angle θ_c for total internal reflection (here the lower core/SiO₂-substrate boundary is of importance only since the refractive index contrast at the upper core/air boundary is high enough to ensure total internal reflection at angles θ safely higher than θ_c). This model was proposed by Khriachtchev et al. [14,15] to explain TE/TM mode structure in Si-NC planar waveguides similar to ours. The spectral separation between TE and TM modes, is then a direct consequence of the asymmetric index profile with different phase shifts expected for the TE and TM modes under total reflection at both boundaries.

- (ii) *Radiative substrate modes*: We have previously proposed an alternative mechanism involving substrate leaking or radiation modes of the Si-NC waveguide [10,11]. These modes propagate at angle θ situated close to but *below* θ_c and undergo total reflection at the upper boundary (larger index difference) but are only partially reflected on the lower boundary (smaller index difference). Consequently, a small fraction of their power is radiated into the substrate at each bottom reflection. If the angle θ is only slightly less than θ_c , the leaking modes propagate near-parallel to the Si-NC plane. Moreover, the number of reflections is very high (R is close to unity), resulting in a narrow spectral width for the modes. The mechanism of spectral filtering in this case remains the same as discussed above, the only difference being that a phase shift at the upper boundary only comes to play during the initial stages of propagation. After a finite number of internal reflections all the radiant power escapes into leaking modes and emerges from the sample facet in a well defined direction, basically parallel to the Si-NC film. This makes such substrate modes virtually indistinguishable from the guided modes. The substrate modes are usually considered undesirable parasitic radiation and thus do not normally receive much attention. Indeed, only in cases where guided modes undergo significant losses (absorption and scattering in the waveguide core and diffraction on the narrow output aperture) do the substrate leaking modes play a dominant role.

The fact that the two above proposed mechanisms have a different dependence on the refractive index difference at the surface provides the basis for testing their validity experimentally. The principle is to change locally the cladding layer refractive index. This was done by placing liquid drops on the waveguide/air surface [11,16]. If a drop is above the excited PL spot, the TE/TM modes gradually red-shift and broaden with increasing refraction index of

applied liquid and eventually disappear if the index contrast approaches zero. However, when the drop is placed some millimeters away from the spot (between the photo-excited spot and the output facet), no changes in modes is observed, consistent with all the radiant power escaping into radiative substrate modes. These experiments are supported by numerical modeling of the PL spectra which show excellent agreement with experiments and provide unambiguous validation of the leaking modes model [11].

3.4. Coupling and propagation of external light in Si-NC waveguides

The transmission spectra of the five samples (implantation fluence $4\text{--}6 \times 10^{17} \text{ cm}^{-2}$) obtained by white-light coupling through a prism (Fig. 1A) are shown in Fig. 6. In the measured spectral region two broad transmission bands (blue and red) are observed for each sample. The positions of both bands red-shifts with increasing fluence and the position of long-wavelength bands coincides with that of the PL leaking modes (Fig. 5A). Our calculation show that the red and blue bands correspond to second and third order leaking modes (the first one being in infrared). Broadening of the mode structure may be a consequence of the very low number of reflections undertaken by coupled light before escaping to the substrate [17].

Coupling of external light (the warm-white LED) through a truncated facet (Fig. 1B) gives the best result for a coupling angle $\gamma \sim 20^\circ$, as expected (Fig. 7). In this configuration we detect narrow and polarization-split peaks at an output angle $\alpha \sim 2^\circ$. The peaks are, however, not transmission but absorption peaks. This can be understood if it is assumed that the detected light is not from radiative substrate modes (which represent a small portion of transmitted light) but from filtered transmitted light propagating almost parallel to the Si-NC waveguide

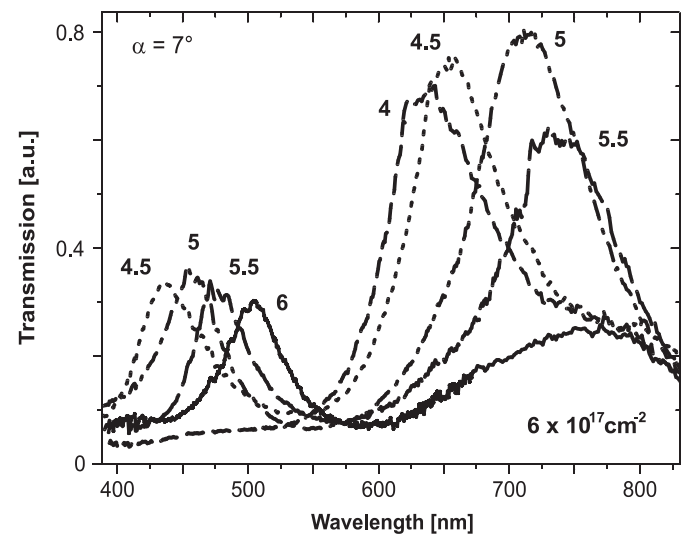


Fig. 6. The transmission spectra of prism-coupled light detected at angle $\alpha = 7^\circ$ from samples presented in Fig. 5.

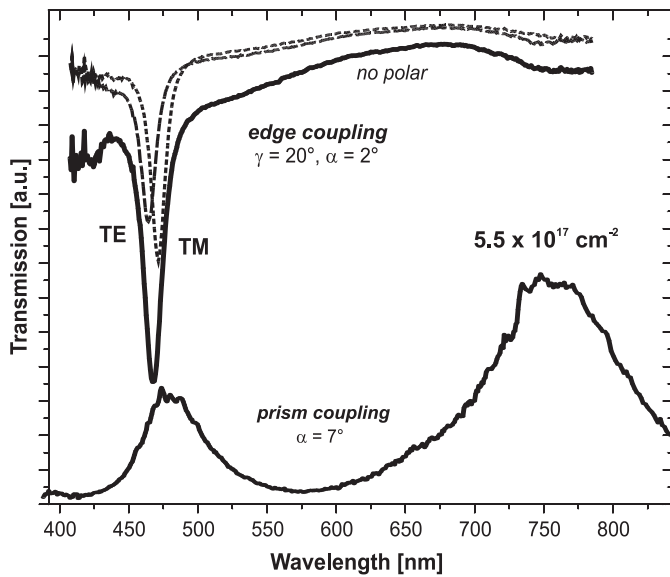


Fig. 7. Comparison of transmission spectra of sample $5.5 \times 10^{17} \text{ cm}^{-2}$ obtained by the direct facet-coupling (upper curves, solid line—no-polarization, dashed and dotted lines correspond to TE and TM polarization, respectively) and by the prism-coupling (lower spectrum).

from which a part of power escaped to the substrate modes. The blue third order modes are much stronger compared to second order because of higher absorption in blue spectral region.

3.5. Leaking modes vs. optical gain

One of the most interesting questions concerning nanocrystal waveguides is the interplay between radiative substrate modes and optical amplification by stimulated emission. Since the first report on optical gain in Si-ion implanted Si-NC layers by Pavese et al. [18] similar samples have been investigated by other groups with both positive [4] and negative [19] results. Two aspects of this problem are addressed here.

First, experimental artefacts have been shown to play an important role when measuring optical gain close to leaking modes maxima by the commonly used variable-stripe-length (VSL) technique [20]. These artefacts are mainly due to unconventional propagation and coupling of these modes in the detection system, and their interplay with the NA of detection. In order to correct most of these artefacts it has previously been proposed that VSL measurements be combined with a shifting-excitation-spot (SES) technique [20]. Indeed, it should be stressed that the interpretation of VSL results without associated SES measurements can lead to erroneous results.

Secondly, the potential advantages of leaking modes for achieving optical gain are spectral narrowing, low losses, and directionality of propagation. On the other hand the propagation path of radiative modes through a pumped active medium (Si-NCs forming the waveguide) is limited by leakage into the substrate. Attempts to achieve optical

gain on leaking modes was successful only under strong nanosecond pulsed pumping (6 ns, 355 nm from THG-Nd:YAG laser) with the gain threshold around 50 mJ/cm^2 and maximum gain at TM mode of about 12 cm^{-1} for 100 mJ/cm^2 excitation [21].

Further theoretical investigation of the radiative modes in the loss/gain medium is in progress.

3.6. Permanent changes of Si-NC waveguides induced by laser pulses

The Si-NC waveguides in silica may be damaged by high-intensity laser excitation and apparent differences in damage are evident for nanosecond and femtosecond pulses. When irradiated with the 420-nm, 5 ns output of an optical parametric oscillator (OPO) pumped by THG-Nd:YAG (NL 303 + PG122, Ekspla) the damage threshold is very sharp at around 800 mJ/cm^2 . The damage appears as micrometer-size granular aggregates in the Si-NC followed immediately by complete ablation of the implanted layer. The mechanism is most probably related to heating and even melting of Si-NCs [22] which leads to failure of the silica matrix. This is evidenced by the appearance of cracks and surface ruptures which can lead to complete removal of the SiNC layer.

In contrast, femtosecond laser excitation (400 fs, 400 nm from SHG-Ti:sapphire laser) starts to modify sample at much lower pulse energies $\geq 20 \text{ mJ/cm}^2$. There are two distinct phases of layer damage. The initial stage appears as darkening (brown coloration) of the excited area. Micro-Raman measurements (not presented here) show that it corresponds to amorphization of the Si-NC layer

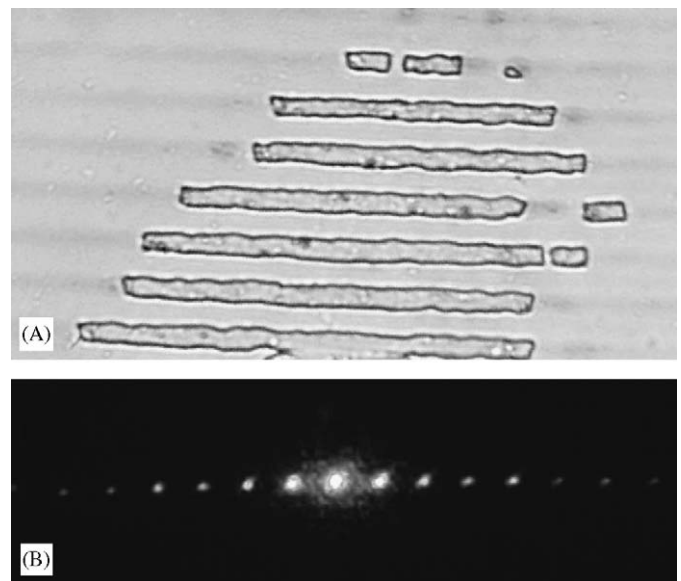


Fig. 8. (A) The diffraction grating (period of about $12 \mu\text{m}$) ablated in the Si-NC waveguide (implanted fluence $4 \times 10^{17} \text{ cm}^{-2}$) by an interfering laser pulses from femtosecond laser (SHG-Ti:sapphire laser, 400 fs, 400 nm). (B) A photograph of the pattern produced by diffraction of 633 nm He-Ne laser beam on the ablated grating.

(it appears similar to the implanted layer before annealing). In the second step at higher excitation the layer is ablated. Clearly, the damage mechanism for ultrashort laser pulses (400 fs) is different to that of the longer (5 ns) pulses. The advantage of fs-ablation is that the boundary between the ablated and unchanged area can be very sharp, enabling fs-laser-ablation to be used for lithography to create microstructures in the planar waveguides. In Fig. 8 we demonstrate a diffraction grating with $12\ \mu\text{m}$ period written into $4 \times 10^{17}\ \text{cm}^{-2}$ implanted layer by 400 fs, 400 nm fs-pulses.

4. Conclusions

Si-ion implantation into silica slabs or oxide layers on Si wafer followed by annealing is a relatively easy way to fabricate active nanocrystalline planar waveguides. In spite of their simplicity these waveguides show rich optical phenomena which are mainly connected to peculiar radiative substrate modes—so-called leaking modes. This study has investigated the influence of these complex propagation modes on PL, transmission, and gain spectra both experimentally and theoretically. Similar anomalous phenomena connected to the interplay between radiative and guided modes are expected to take place in other types of active waveguides. The possibility of spectral, polarization, and spatial filtering reported for active Si-NC waveguides offer interesting possibilities for application in silicon-based photonic devices or sensors.

Acknowledgement

Financial support through the projects of Research plan MSM0021620835 and Research centre LC510 of MSMT CR, Project no. IAA1010316 of GAAV CR, 202/01/D030 of GACR, the Australian Research Council, and a grant of the Lithuanian State Foundation for Science and Studies (R.T.) is greatly acknowledged. The research work at the Institute of Physics is supported by Institutional Research Plan no. AV0Z 10100521. One of the authors (I.P.) thanks the Laserlab-Europe Integrated Initiative for financial support (vulrc001168).

References

- [1] S. Ossicini, L. Pavesi, F. Priolo (Eds.), *Light Emitting Silicon for Microelectronics*, vol. 194, Springer, Berlin, 2003 Springer Tracts in Modern Physics.
- [2] A. Irrera, D. Pacifici, M. Miritello, G. Franzo, F. Priolo, F. Iacona, D. Sanfilippo, G. Di Stefano, P.G. Fallica, *Appl. Phys. Lett.* 81 (2002) 1866.
- [3] R.J. Walters, G.I. Bourianoff, H.A. Atwater, *Nature Mater.* 4 (2005) 143.
- [4] L. Khriachtchev, M. Räsänen, S. Novikov, J. Sinkkonen, *Appl. Phys. Lett.* 79 (2001) 1249.
- [5] J. Valenta, I. Pelant, K. Luterová, R. Tomasiunas, S. Cheylan, R.G. Elliman, J. Linnros, B. Hönerlage, *Appl. Phys. Lett.* 82 (2003) 955.
- [6] L. Dal Negro, M. Cazzanelli, N. Daldosso, Z. Gaburro, L. Pavesi, F. Priolo, D. Pacifici, G. Franzo, F. Iacona, *Physica E* 16 (2003) 297.
- [7] M. Cazzanelli, D. Navarro-Urrios, F. Riboli, N. Daldosso, L. Pavesi, J. Heitmann, L.X. Yi, R. Scholz, M. Zacharias, U. Gösele, *J. Appl. Phys.* 96 (2004) 3164.
- [8] L. Khriachtchev, M. Räsänen, S. Novikov, J. Lahtinen, *J. Appl. Phys.* 95 (2004) 7592.
- [9] J. Valenta, T. Ostatnický, I. Pelant, R.G. Elliman, J. Linnros, B. Hönerlage, *J. Appl. Phys.* 96 (2004) 5222.
- [10] T. Ostatnický, J. Valenta, I. Pelant, K. Luterová, R.G. Elliman, S. Cheylan, B. Hönerlage, *Opt. Mater.* 27 (2005) 781.
- [11] I. Pelant, T. Ostatnický, J. Valenta, K. Luterová, E. Skopalová, T. Mates, R.G. Elliman, *Appl. Phys. B* 83 (2006) 87.
- [12] H.G. Unger, *Planar Optical Waveguides and Fibres*, Clarendon Press, Oxford, 1977.
- [13] H. Kogelnik, V. Ramaswamy, *Appl. Opt.* 13 (1974) 1867.
- [14] L. Khriachtchev, M. Räsänen, S. Novikov, *Appl. Phys. Lett.* 83 (2003) 3018.
- [15] L. Khriachtchev, S. Novikov, J. Lahtinen, M. Räsänen, *J. Phys. Condens. Matter* 16 (2004) 3219.
- [16] K. Luterová, E. Skopalová, I. Pelant, M. Rejman, T. Ostatnický, J. Valenta, *J. Appl. Phys.*, accepted for publication.
- [17] P. Janda, J. Valenta, T. Ostatnický, I. Pelant, R.G. Elliman, *Thin Sol. Films* (in press).
- [18] L. Pavesi, L. Dal Negro, C. Mazzoleni, G. Franzo, F. Priolo, *Nature* 408 (2000) 440.
- [19] R.G. Elliman, M.J. Lederer, N. Smith, B. Luther-Davies, *Nucl. Instrum. Meth. Phys. Res. B* 206 (2003) 427.
- [20] J. Valenta, I. Pelant, J. Linnros, *Appl. Phys. Lett.* 81 (2002) 1396.
- [21] K. Luterová, D. Navarro, M. Cazzanelli, T. Ostatnický, J. Valenta, S. Cheylan, I. Pelant, L. Pavesi, *Phys. Status Solidi (c)* 2 (2005) 3429.
- [22] B.V. Kamenev, H. Grebel, L. Tsybeskov, *Appl. Phys. Lett.* 88 (2006) 143117.